



Cite this: *Phys. Chem. Chem. Phys.*,
2018, 20, 27205

Monitoring *cis*-to-*trans* isomerization of azobenzene using terahertz time-domain spectroscopy

Lu Zhou,^{†a} Ligang Chen,^{†a} Guanhua Ren,^{†a} Zhongjie Zhu,^b Hongwei Zhao,^{ib}
Huabin Wang,^c Weili Zhang^{ib}*^{ad} and Jiaguang Han^{ib}*^a

We present terahertz time-domain spectroscopy (THz-TDS) to explore the conformational dynamics of thermally induced and photoinduced isomerization of azobenzene. The essence of the method is that isomerization of azobenzene proceeds *via* large structural changes in the molecule, while the THz response is sensitive to these changes. We experimentally demonstrate that the THz spectra of azobenzene show remarkable variations upon heating and irradiation, and as such quantitatively recorded and identified THz spectroscopy can be used to monitor the isomerization process. Specifically, the measured THz spectra clearly reveal that the rate of thermal-isomerization from *cis*-to-*trans* in non-polar solvents is faster than that in polar solvents, and an about 6-fold acceleration of the rate could be achieved when Au NPs were introduced as a catalyst into azobenzenes. Moreover, we provide evidence that the temperature and Au NP catalyst do not have an obvious influence on the photoinduced isomerization of azobenzene. The presented example illustrates the power of the THz-TDS method to open up a novel avenue for exploring molecular dynamics.

Received 19th July 2018,
Accepted 9th October 2018

DOI: 10.1039/c8cp04570d

rsc.li/pccp

Introduction

Azobenzene (AB), a diazene (HN=NH) derivative, which consists of two benzene rings joined by a N=N double bond, can exist in either the *cis* or *trans* conformation. When irradiated with ultraviolet (UV) or visible (vis) light, the isomerization from the stable *trans* to the metastable *cis* is induced, and the reverse process can occur either by irradiating or heating.^{1,2} This reversible geometric effect was first noted in 1937 by Hartley,³ when he observed the *cis* isomer of AB upon irradiation. Since then, the isomerization of AB has attracted intense interest because of its potential applications in optical switches,^{4–6} memory storage,^{7,8} molecular machines,^{9,10} and light-sensitive biomolecules.^{11,12} The isomerization processes of AB have been monitored and characterized by a variety of

methods including UV-vis absorption, Raman, nuclear magnetic resonance (NMR), and so on. For example, Quick *et al.*¹³ studied the photo-isomerization dynamics and pathways of *cis*- and *trans*-AB in solution by using UV-vis absorption. The excited-state structure and dynamics of *cis*- and *trans*-AB were investigated by Stuart *et al.*,¹⁴ where the method of resonance Raman was adopted. Curtis *et al.*¹⁵ obtained the nitrogen-15 NMR spectra of AB. The previous reported methods can monitor the thermal- or photo-isomerization of AB well, and thus play important roles in the studies of AB. However, of particular note, it is well known that AB is sensitive to light, and the above methods unavoidably cause additional irradiation of AB. Therefore, developing new approaches with minimum interference to quantitatively monitor the conformational dynamics of isomerization of AB holds great promise in determining the course of chemical reactions and thus enabling novel applications.

Terahertz time-domain spectroscopy (THz-TDS), containing abundant physical and chemical information on materials, has shown many promising applications in the fields of physics,¹⁶ chemistry,¹⁷ materials science¹⁸ and biology.¹⁹ As a non-destructive data acquisition and coherence detection technology, THz-TDS provides a reliable and unique analytical method to study the characteristics of molecules. In particular, the low-frequency torsional vibration or rotation energy levels of most molecules lie in the THz region, and low-frequency vibrational or rotational THz spectroscopy is highly sensitive to the conformation and structure

^a Center for Terahertz Waves and College of Precision Instrument and Optoelectronics Engineering, Tianjin University, Tianjin 300072, China.
E-mail: weili.zhang@okstate.edu, jiaguan@tju.edu.cn

^b Shanghai Institute of Applied Physics, Chinese Academy of Sciences, Shanghai 201800, P. R. China

^c Chongqing Engineering Research Center of High-Resolution and Three-Dimensional Dynamic Imaging Technology, Chongqing Institute of Green and Intelligent Technology, Chinese Academy of Science, Chongqing 400714, China

^d School of Electrical and Computer Engineering, Oklahoma State University, Stillwater, Oklahoma 74078, USA

[†] These authors contributed equally to this work.

of molecules. Therefore, the high sensitivity of THz spectroscopy provides us with a powerful and unique fingerprint to probe the conformational dynamics of molecules. A major difference between THz-TDS and Raman or UV-vis spectroscopy is that THz-TDS is a coherent measurement process, in which one could directly obtain the optical parameters of a sample such as refractive index and dielectric constants.^{20,21} Another significant advantage of the use of THz-TDS is that THz waves do not give rise to direct electronic excitations in the sample and therefore avoid causing damage or other photochemical reactions due to their low photon energies and non-ionization.

Thermal- or photo-isomerization of AB proceeds *via* large structural changes and THz spectroscopy is thus very useful to monitor these dynamical processes. In light of that, herein, we apply the THz-TDS method to quantitatively monitor the *cis-trans* isomerization of AB. The quantitative thermally induced *cis-to-trans* isomerization of AB in different polar solvents and under gold nanoparticle (Au NP) catalysis was characterized by THz-TDS. Our measured results demonstrate that the rate of thermal *cis-to-trans* isomerization of AB in non-polar solvent is faster than that in polar solvent. The thermal *cis-to-trans* isomerization reaction of AB is highly accelerated when Au NPs are introduced as a catalyst. Moreover, the photoinduced isomerization of AB from *cis-to-trans* under different conditions was also investigated by THz-TDS. It was found that the temperature and catalyst have no remarkable influence on the photo-isomerization of AB.

Experimental

Chemicals

trans-Azobenzene (*trans*-AB) was purchased from J&K Scientific Co., Ltd. The *cis*-azobenzene (*cis*-AB) was obtained by illuminating an ethanol solution of *trans*-AB with an ultraviolet lamp (consumed power 250 W) at 365 nm. About 40% of *cis*-AB was produced within two hours then purified by column chromatography with silica gel (200 mesh) as the stationary phase and petroleum ether and ethyl acetate mixed solvent (40:1, v/v) as eluents. COC (cyclic olefin copolymer) powder (particle size 50–70 μm) was purchased from Terahertz Photonics Co., Ltd. Acetone, tetrachloromethane (CCl₄), ethanol and *n*-hexane were obtained from Real and Lead Chemical Co., Ltd. Hydrogen tetrachloroaurate(III) trihydrate (HAuCl₄·3H₂O) was purchased from Sigma-Aldrich. Trisodium citrate (Na₃C₆H₅O₇·2H₂O) was purchased from Aladdin.

Synthesis of Au nanoparticles

Au nanoparticles (Au NPs) with an average radius of 20 nm were prepared according to the procedure developed by Turkevich *et al.*²² 2 mL (1%) sodium citrate aqueous solution was added immediately to 100 mL of a 10⁻⁴ g mL⁻¹ HAuCl₄ boiling solution under vigorous stirring. The mixture was stirred vigorously and boiled for an additional 20 min. Then the obtained Au colloids were purified by 3 cycles of re-dispersion in ethanol and centrifugation at 12 000 rpm for 15 min.

Finally, the Au NPs were obtained and stored at -4 °C for further use.

Thermally induced *cis-to-trans* isomerization of AB

Thermally induced *cis-to-trans* isomerization of AB was performed as follows. The 0.14 M solutions (8 mL) of *cis*-AB in different solvents (ethanol, acetone, *n*-hexane and CCl₄) were prepared and then the solutions in closed brown bottles were kept in a water bath at a temperature of 50 °C for a certain time interval. After the allotted time, the solid powder of AB was obtained in a gentle flow of dry air at room temperature for THz measurement.

In addition, Au NP catalyzed thermally induced *cis-to-trans* isomerization of AB in ethanol solution was also performed. Similarly, 300 μL of the Au NP colloid was added into the 0.14 M (8 mL) *cis*-AB (in ethanol solution) in a brown bottle and the mixed solution was kept in a water bath at 50 °C for a certain time interval. Then, the mixture was washed by centrifugation at 12 000 rpm for 15 min to remove the Au NP colloid. Afterwards, the solid powder of AB was obtained in a gentle flow of dry air at room temperature for THz measurement.

Photoinduced isomerization of AB from *cis-to-trans*

The photoinduced isomerization of AB from *cis-to-trans* under different conditions was carried out and the steps of the experiment are similar to the above procedure for thermal-isomerization. Briefly, 0.14 M *cis*-AB in different solvents (ethanol, acetone, *n*-hexane and CCl₄) was irradiated with visible light at 445 nm (210 mW) for a certain time interval under vigorous stirring at room temperature and 50 °C. Then the solid powder of AB was obtained, in a gentle flow of dry air at room temperature for THz measurement.

In addition, Au NP catalyzed photo-isomerization of AB from *cis-to-trans* in ethanol solution was also performed. Similarly, 300 μL of the Au NP colloid was added into the 0.14 M (8 mL) *cis*-AB (in ethanol) solution in a closed beaker and the mixed solution was irradiated at room temperature for a certain time interval. Then, after the allotted time, the mixture was washed by centrifugation at 12 000 rpm for 15 min to remove the Au NP colloid. Afterwards, the solid powder of AB was obtained, in a gentle flow of dry air at room temperature, for THz measurement.

Sample preparation

For the THz-TDS measurements, the powder AB samples were pressed into disks with a hydraulic press at a pressure of 15 MPa. The thickness of the sample tablets was approximately 0.7 mm, and the diameter was 13 mm. As for the low temperature experiments, the AB powder was blended with COC powder, which was nearly transparent in the THz region, at a mass ratio of 1:3 (50 mg:150 mg) and then pressed into disks of 1.4 mm thickness.

Instrumentation

UV-vis absorption spectra were measured with a spectrometer (TU1901, Pgeneral). An SU-70 FESEM instrument was used to

record the scanning electron microscopy (SEM) images under an accelerating voltage of 5 kV. Powder X-ray diffraction (PXRD) patterns of *cis*- and *trans*-AB were recorded using an X'Pert Pro MPD (Cu source, 40 kV voltage, 40 mA filament emission). The data were collected over a scan range from 10° to 40° (2 θ). Photo-isomerization of AB was achieved using a diode pumped solid state laser (DPSSL, 210 mW, Shanxi Tongwei Optoelectronic Equipment Co., Ltd.) with a wavelength of 445 nm.

Quantum chemical calculations

Calculations based on DFT using the Cambridge Sequential Total Energy Package (CASTEP) program as a part of the Materials Studio package from Accelrys were performed to analyze the observed THz spectra. After verification by comparing measured PXRD spectra (see insets of Fig. 2(a and d)) of the samples with those calculated from the previous data published, crystal cell parameters of *trans*- and *cis*-AB for calculations were taken from ref. 23 and 24 respectively. The *trans*-AB belongs to the monoclinic crystal system, and the space group is $P2_1/a$ ($Z = 4$), with lattice dimensions of $a = 12.144 \text{ \AA}$, $b = 5.756 \text{ \AA}$, $c = 15.396 \text{ \AA}$, $\alpha = 90^\circ$, $\beta = 114^\circ 8'$, $\gamma = 90^\circ$. The *cis*-AB is suggested to be orthorhombic in structure with the space group $Pbcn$ ($Z = 4$), and the corresponding lattice parameters are $a = 7.57 \text{ \AA}$, $b = 12.71 \text{ \AA}$, $c = 10.32 \text{ \AA}$, $\alpha, \beta, \gamma = 90^\circ$. The calculations were performed on the crystalline state within the generalized gradient approximation (GGA) at the Perdew–Burke–Ernzerhof (PBE) correlation functional. Grimme's dispersion-corrected method was used for DFT-D correction and norm-conserving pseudopotential for CASTEP.

THz-TDS measurements

The measurements were performed with two THz-TDS systems, one is a photoconductive switch-based 8-F confocal THz-TDS system,²⁵ the other is a TAS7400TS THz-TDS system (Advantest Corporation, Japan), which is used for the low temperature experiments in this work. The effective spectrum band is 0.2 to 2.5 THz. The THz beam pathway was purged with dry air to keep a relative humidity of about 2.5%. We extracted the absorption coefficient, refractive index and complex dielectric function of the samples from their transmitted THz pluses.

Temperature-dependent THz spectra of AB were measured using a temperature controller (Specac Ltd UK, accuracy $\pm 0.5^\circ \text{C}$) which is equipped with COC windows. THz spectra were recorded over the temperature range from -190 to 22°C (83–295 K).

Results and discussion

THz spectra of AB

Fig. 1 shows the THz power absorption coefficient α , refractive indices n , and complex dielectric functions ϵ , of *trans*- and *cis*-AB in the range of 0.2–2.5 THz at room temperature. *trans*-AB has two distinct absorption peaks at 1.39 and 1.74 THz, and a shoulder peak at 2.28 THz. *cis*-AB has four obvious absorption peaks located at 0.6, 0.9, 1.27 and 2.19 THz. It is found that the absorption coefficient of the *trans*-AB is extremely low, and is

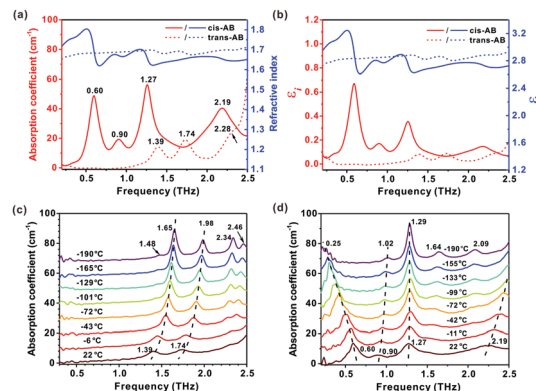


Fig. 1 (a) The THz absorption spectra and refractive index of *trans*- and *cis*-AB and (b) the corresponding complex dielectric functions. The temperature effect on the THz absorption spectra of (c) *trans*-AB and (d) *cis*-AB.

less than 3 cm^{-1} below 1.0 THz and then gradually increases with increasing frequency. The corresponding refractive index shows a comparatively smooth feature at a value of about 1.7 in our measured frequency range. Below 2.3 THz, the *cis*-AB has a much higher absorption coefficient than *trans*-AB, especially at the absorption peaks of 0.60 and 1.27 THz. Fig. 1(b) shows the real part ϵ_r and imaginary part ϵ_i of the measured complex dielectric functions of all samples, where the frequency-dependent complex dielectric function is obtained through the formula:²⁶ $\epsilon_r = n_r^2 - (a\lambda_0/4\pi)^2$ and $\epsilon_i = \alpha n_r \lambda_0 / 2\pi$.

Additionally, we measured the THz spectra of the two isomers within a temperature range ranging from -190 to 22°C . For *trans*-AB, as shown in Fig. 1(c), the absorption peaks become stronger and sharper and suffer a distinct blue-shift with the decrease of temperature. The two peaks at 1.39 and 1.74 THz were blue-shifted to 1.65 and 1.98 THz, respectively. Such a shift is usually ascribed to the increased bond length due to thermal expansion.²⁷ Meanwhile, the shoulder peak at 2.28 THz split into two peaks at 2.34 THz and 2.46 THz, and a weak peak at 1.48 THz gradually appeared. The *cis*-AB shows similar behaviors to the *trans*-AB. The absorption peaks became stronger with decreasing temperature, and then two small peaks appeared at 1.64 and 2.09 THz at low temperature. We also noticed that as the temperature decreased, the peak at 0.6 THz has a significant red-shift rather than a blue-shift like other peaks, and the peak at 1.27 THz shows a negligible frequency shift. The intensities and frequency positions of peaks usually show a temperature dependent change in the THz spectrum.^{28–31} The stronger and sharper peaks are the result of temperature-dependent changes in distribution of the energy vibrational states.²⁸ The temperature induced frequency shifts have been considered as the consequence of multiple mechanisms. The origins of the blue shift for most peaks are the anharmonicity of vibrational potential and the temperature-dependent change of the volume.^{28,29,32} The anomalous red shift at 0.60 THz can be interpreted as the interaction of weak intermolecular bonding forces such as hydrogen bonds and van der Waals forces.³² The behaviour seen at 1.27 THz, almost unchanged

with temperature, can be explained by the combination of two effects which lead to opposite frequency shifts.

Quantum chemical calculation of *trans*- and *cis*-AB

Quantum chemical calculations were performed to understand the experimentally measured THz responses of AB. The simulated THz spectra of *trans*- and *cis*-AB using solid-state DFT calculations are plotted in Fig. 2(a and d), where the simulated results are overall in good agreement with the experimental ones. Four typical vibrational modes of *trans*- and *cis*-AB are demonstrated in Fig. 2(b–f). For *trans*-AB, four molecules are arranged in the unit cell with space group symmetry $P2_1/a$, with the centers of each molecule lying on a center of symmetry of the lattice. According to ref. 23, the molecules centered on (0, 0, 0) and those centered on (0, 0, 1/2) are non-equivalent, and this non-equivalent property has also been reflected in the calculated vibrational modes as shown in Fig. 2. The experimental peak at 1.65 THz corresponds to the vibrational mode calculated at 1.44 THz, primarily arising from the translation of molecules centered on (0, 0, 0) along with milder translation of molecules on (0, 0, 1/2). The measured peak at 1.98 THz is relative to the calculated peak at 2.00 THz, arising from the twisting of the benzene rings with translation of the N=N bond of the molecules centered on (0, 0, 1/2) while the molecules centered on (0, 0, 0) show a negligible translation. For *cis*-AB, the peak at 0.6 THz at room temperature, which takes a significant red-shift with decreasing temperature, can be attributed to the calculated mode at 0.39 THz, due to the rotational vibration of the whole molecule (Fig. 2(e)). The mode at 1.60 THz originates from the translation along with the rotation of the molecules. Table 1 gives the detailed descriptions of the vibrational modes of *trans*- and *cis*-AB.

The THz absorption spectra for mixtures of *cis*- and *trans*-AB

To quantitatively study the isomerization process of AB from *cis*-to-*trans*, the THz absorption spectra of different ratios of

cis- and *trans*-AB mixtures were plotted in Fig. 3(a). On decreasing the content of *cis*-AB, the absorption peaks of *cis*-AB at 0.6, 0.9, 1.26 and 2.20 THz decrease before vanishing, and meanwhile the peaks of *trans*-AB at 1.39 and 1.74 THz emerge and increase gradually. Particularly, the peaks at 0.6 THz exhibit a clean gradient change process upon decreasing the content of *cis*-AB. As such, the peak at 0.6 THz was used to evaluate the content of *cis*-AB in the two isomers. The dose–response fit curve of the peak intensity at 0.6 THz for different ratios of *cis*-AB shown in Fig. 3(b) obeys the linear regression equation: $y = -0.95 + 0.45x$, correlation coefficient $R^2 = 0.997$. From the dose–response, the absorption coefficient of the designated peak was proportional to the *cis*-AB content in mixtures across the whole range.

Thermally induced *cis*-to-*trans* isomerization of AB

The thermally induced *cis*-to-*trans* isomerization process of AB in different polarity solvents (ethanol, acetone, hexane and CCl_4) at 50 °C was monitored by using the THz-TDS method. Fig. 4(a) illustrates the THz absorption spectra of the thermal *cis*-to-*trans* isomerization process of AB in ethanol solution at 50 °C. Upon heating, the metastable *cis*-AB is isomerized into the thermostable *trans*-AB. The THz absorption peaks of the *cis*-AB at 0.6, 0.9, 1.26 and 2.20 THz decrease with increasing heating time. Meanwhile, the new peaks at 1.39 and 1.74 THz emerge after 4 h and then become stronger with heating time. After 38 h, the peaks for *cis*-AB vanished and the peaks for *trans*-AB reached to the maximum. It means that the *cis*-AB was thermally-isomerized to *trans*-AB. Similarly, Fig. 4(b) shows the THz absorption spectra of the thermal *cis*-to-*trans* isomerization process of AB in polar solvent (acetone). In Fig. 4(b), the THz absorption peaks of the *cis*-AB at 0.6, 0.9, 1.26 and 2.20 THz gradually decrease until they disappear after 38 h. The THz absorption peaks of *trans*-AB at 1.39 and 1.74 THz appeared and reached

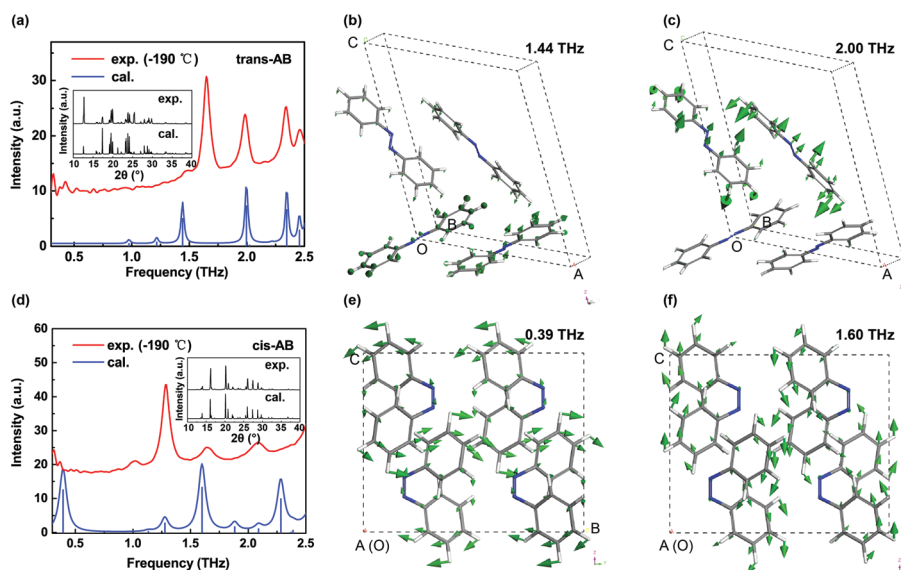


Fig. 2 (a) The experimental and calculated THz spectra of *trans*-AB, the inset is the measured and calculated PXRD result; the simulated vibrational modes of *trans*-AB at (b) 1.44 and (c) 2.00 THz. (d–f) The corresponding results of *cis*-AB.

Table 1 Calculated vibrational modes and corresponding experimental peaks of AB^a

Isomer	Exp. (THz)		Cal. (THz)	Vibrational mode
	22 °C	−190 °C		
<i>trans</i> -AB			0.98	Wagging of benzene ring of $M_{1/2}$, translation of M_0
		1.48	1.22	Wagging of benzene ring of $M_{1/2}$, translation of M_0
	1.39	1.65	1.44	Translation of M_0 , weaker translation vibration of $M_{1/2}$
	1.74	1.98	2.00	Twisting of benzene ring with translation of N=N bond of $M_{1/2}$, translation of M_0
	2.28	2.35	Rotation of benzene ring of $M_{1/2}$, twisting of benzene ring with translation of N=N bond of M_0	
<i>cis</i> -AB	0.6	0.25	0.39	Rotation
	0.9	1.02	1.28	Rotation perpendicular to benzene ring
	1.27	1.29	1.60	Rotation along with translation
		1.64	1.88	Rotation
		2.09	2.09	Twisting of benzene ring and translation of N=N
	2.19	> 2.5	2.28	Rotation

^a M_0 stands for the molecules centered on (0, 0, 0), $M_{1/2}$ stands for the molecules centered on (0, 0, 1/2).

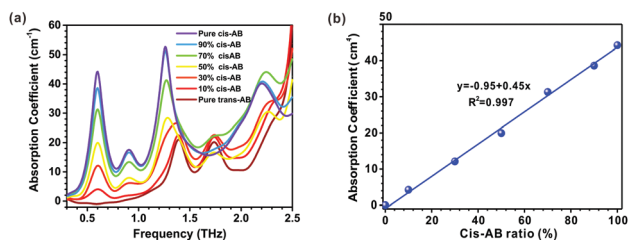


Fig. 3 (a) The THz absorption spectra of the mixtures composed of different ratios of *cis* and *trans*-AB. (b) Plot of the absorption coefficient versus the ratio of *cis* and *trans*-AB in the mixture at 0.6 THz.

their maximum at 38 h, indicating that the *cis*-AB is completely isomerized into the *trans*-AB. Additionally, the THz absorption spectra of the thermal *cis*-to-*trans* isomerization process of AB in non-polar solvents (hexane and CCl₄) were also explored and are depicted in Fig. 4(c and d), respectively. It can be seen that the absorption peaks of *cis*-AB at 0.6, 0.9, 1.26 and 2.20 THz

decrease with increasing heating time. These changes are accompanied with two new enhanced absorption peaks at 1.39 and 1.74 THz, which emerge after 1h. After 20 h, the peaks of *cis*-AB vanished and the peaks of *trans*-AB reached their maximum. Compared to that in polar solvent (Fig. 4(a and b)), the isomerization rate of AB in non-polar solvents is much faster.

To illustrate the solvent polarity-dependent thermal-isomerization rate of AB from *cis*-to-*trans*, the quantitative relationship between the content of *cis*-AB and isomerization time (Fig. 4(f)) was given by measuring the THz absorption spectra of different ratios of *cis* and *trans*-AB mixtures as a standard curve (Fig. 3(b)). From Fig. 4(f), it can be seen that the *cis*-AB content decreased with increasing thermal-isomerization time in polar solvents (ethanol and acetone), and the *cis*-AB content is almost close to 0 at 38 h. However, a similar conversion process in non-polar solvents (hexane and CCl₄) only takes around 20 h. The measured results indicate that the thermal isomerization reaction of AB is dependent on the

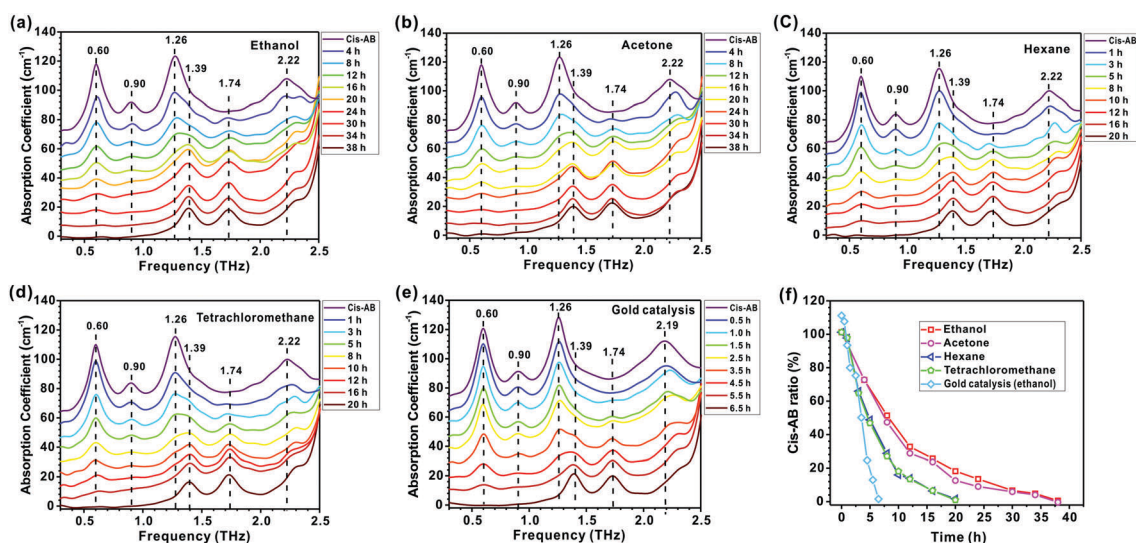


Fig. 4 THz absorption spectra of AB during thermal *cis*-to-*trans* isomerization in different polarity solvents (a) ethanol, (b) acetone, (c) hexane and (d) CCl₄; (e) THz absorption spectra of AB during thermal *cis*-to-*trans* isomerization in ethanol under Au NP catalysis; (f) the ratio of *cis*-AB as a function of thermal-isomerization time.

polarity of the solvent, and that the rate in the non-polar solvent is faster than that in the polar solvent. The reasons for this are currently not quite clear.^{33,34} It is known that the thermal isomerization of AB has two widely recognized major mechanisms: rotation and inversion.¹ We consider that the rotation is the prevalent mechanism in polar solvents, while inversion generally occurs in non-polar media.^{35,36} Theoretical calculations predict a significantly larger activation energy for rotation (36.2 kcal mol⁻¹) as compared to inversion (24.9 kcal mol⁻¹).³⁷ Thus, the rate of thermal isomerization of AB in the non-polar solvent is faster than that in the polar solvent. Certainly, verifying this interpretation needs further investigation, and a full understanding of this effect requires extensive theoretical and experimental work.

So far, we have seen that the thermally induced isomerization could be monitored quantitatively by the THz-TDS method, although the heat-responsive conversion time is long. As such, we explored the catalytic effect of Au NPs upon the thermally induced *cis*-to-*trans* isomerization of AB. As shown in Fig. 4(e), it can be found that the THz absorption peaks of *cis*-AB at 0.6, 0.9, 1.26 and 2.22 THz gradually decrease and then completely disappear after 6.5 h. Meanwhile, the absorption peaks of *trans*-AB at 1.74 and 1.39 THz appeared and reached their maximum at 6.5 h. The quantitative relationship between the content of *cis*-AB and isomerization time was also investigated in Fig. 4(f). The content of *cis*-AB decreases with increasing thermal-isomerization time under Au NP catalysis and is almost down to 0 after 6.5 h. The measured results show clearly that the rate of thermal *cis*-to-*trans* isomerization of AB is significantly accelerated in the presence of Au NPs. Compared to that in the absence of Au NPs, a nearly 6-fold acceleration in the thermal *cis*-to-*trans* isomerization of AB is achieved. It is ascribed to the participation of Au NP-mediated electron transfer in the thermal isomerization of AB, in which Au NPs mediate electron transfer in the isomerization, followed by AB

radical cation formation and rotation about an activated N=N bond.^{38,39} It is worth noting that the effect of Au NPs in different solvents on catalysis is not given here because the as-prepared Au NPs are hardly dispersed and were inclined to agglomerate together in other solvents.

Photoinduced isomerization of AB from *cis*-to-*trans* at room temperature

The photoinduced *cis*-*trans* isomerization of AB irradiated with visible (445 nm laser) light in polar (ethanol and acetone) and non-polar (hexane and CCl₄) solvents at room temperature was studied. Fig. 5(a) shows the THz absorption spectra of the vis-induced *cis*-to-*trans* isomerization in ethanol solution. It can be seen that the THz absorption peaks of *cis*-AB at 0.6, 0.9, 1.26, and 2.22 THz decreased with increasing irradiation time and meanwhile the absorption peaks of *trans*-AB at 1.74 and 1.39 THz emerged at 45 min and then increased gradually with increasing irradiation time. Subsequently, the absorption peak of *cis*-AB at 0.9 THz vanished, and the absorption peak at 1.26 THz was obscured by the peak of *trans*-AB at 1.39 THz at around 90 min. After 90 min, the THz absorption spectra have no obvious changes and the irradiation of the *cis*-AB in ethanol solution produced the photo-stationary state composed of mixtures of *cis*- and *trans*-AB, as shown in Fig. 5(a). Fig. 5(f) depicts the corresponding changes in the content of constituent *cis*-AB at different irradiation times: 94% at 15 min, 62% at 30 min, 43% at 45 min, 29% at 60 min, 20% at 90 min and 19% at 150 min.

Furthermore, Fig. 5(b) shows the THz absorption spectra of the photo-isomerization process of AB in acetone solutions. Likewise, the THz absorption peaks of *cis*-AB decreased and the absorption peaks of *trans*-AB appeared and increased with irradiation time. After 90 min, the absorption peak at 0.9 THz of *cis*-AB disappeared, and the THz absorption of 0.6, 1.39 and 1.74 THz were invariant and photo-isomerization of AB reached

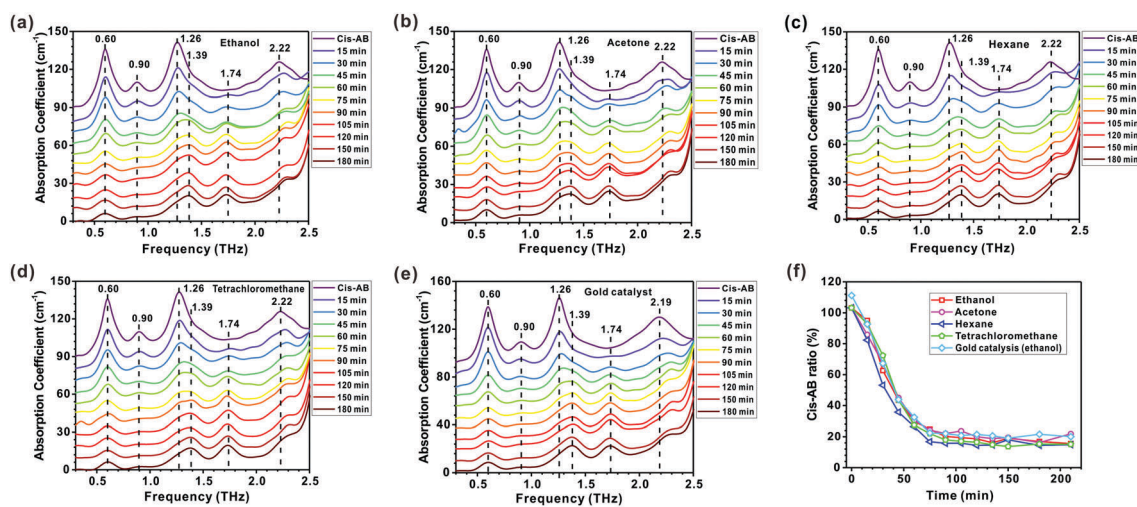


Fig. 5 THz absorption spectra of photo-isomerization of AB from *cis*-to-*trans* in different polarity solvents (a) ethanol, (b) acetone, (c) hexane and (d) CCl₄; (e) THz absorption spectra of photo-isomerization of AB from *cis*-to-*trans* in ethanol under Au NP catalysis; (f) the ratio of *cis*-AB as a function of the photo-isomerization time.

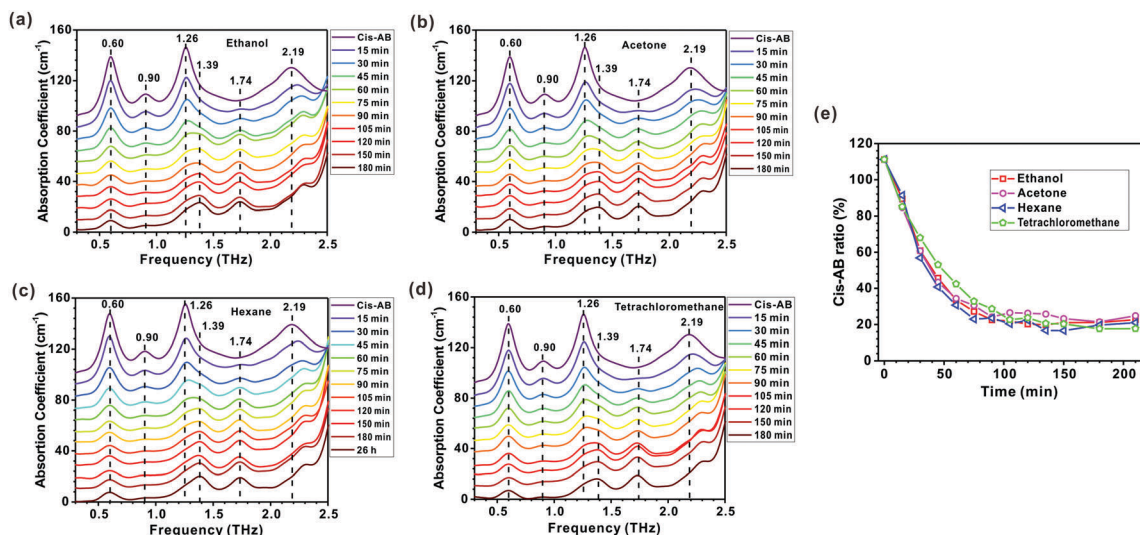


Fig. 6 THz absorption spectra of AB in photo-isomerization from *cis*-to-*trans* at 50 °C in different polarity solvents (a) ethanol, (b) acetone, (c) hexane and (d) CCl_4 ; (e) the ratio of *cis*-AB as a function of the thermal-isomerization time.

the photo-stationary state. In addition, the THz absorption spectra of the photo-isomerization process of AB from *cis*-to-*trans* in non-polar solvents (hexane and CCl_4) were plotted in Fig. 5(c and d), respectively. Similarly, the whole THz absorption spectra of the AB were almost invariant after 90 min of irradiation. Compared to that in polar solvent, the photoinduced conversion of AB from *cis*-to-*trans* shows no significant difference in non-polar solvents. The quantitative relationship between the content of *cis*-AB and irradiation time is given in Fig. 5(f). We observed that the content of the *cis*-AB decreased and then approached asymptotically the same photo-stationary composition ($20 \pm 5\%$ of *cis*-AB) with increased irradiation time in the four solvents at room temperature. It means that the same photo-isomerization equilibrium is established between the *cis*- and *trans*-isomers in different polarity solvents, which indicated that the effect of solvents on photo-isomerization of AB from *cis*-to-*trans* is almost negligible.^{40,41}

Additionally, studies of Au NP catalysis on the photoinduced isomerization of AB from *cis*-to-*trans* in ethanol solution at room temperature were carried out. As shown in Fig. 5(e), with Au NPs, the overall THz absorption spectra of the AB display very similar behaviors to those without Au NPs, as well as the quantitative relationship between *cis*-AB content and reaction time (Fig. 5(f)). Therefore, the *cis*-AB content during the photo-isomerization process, in the absence or presence of Au NPs, was coincident and the Au NPs do not play a catalytic role in the photo-isomerization process. According to the literature,⁴² the catalyst is not responsible for the photo-isomerization of AB.

Photoinduced isomerization of AB from *cis*-to-*trans* under heating

The THz absorption spectra of the photo-isomerization process of AB from *cis*-to-*trans* irradiated with visible light at 50 °C in the above four solvents were also measured. Fig. 6(a) gives the THz absorption spectra of the isomerization process of AB from *cis*-to-*trans* in ethanol solution. It can be seen that the THz absorption

peaks of *cis*-AB at 0.6, 0.9, 1.26 and 2.20 THz decrease and meanwhile the peaks of *trans*-AB at 1.39 and 1.74 THz emerged and increased gradually with time. The whole THz absorption spectra of the AB became invariant after 90 min of irradiation under heating. Fig. 6(b-d) show the isomerization of AB from *cis*-to-*trans* in acetone, hexane and CCl_4 solutions at 50 °C, respectively. Similarly, the THz absorption peaks of *cis*-AB at 0.6, 0.9, 1.26 and 2.20 THz decrease and meanwhile the peaks of *trans*-AB at 1.39 and 1.74 THz emerged and increased gradually with increasing isomerization time. The THz absorption spectra of the AB are invariant after 90 min of irradiation. To further confirm the effects of temperature on the photoreaction rate and the photo-stationary state of AB, we prolong the irradiation time of *cis*-AB in hexane solution to 26 h at 50 °C, as shown in Fig. 6(c). It can be seen that the THz absorption spectrum of the AB under irradiation for 26 h is consistent with that under 90 min. This indicates that the photo-isomerization of AB from *cis*-to-*trans* can establish a photo-stationary state after 90 min. The quantitative relationship between the content of *cis*-AB and isomerization time was plotted in Fig. 6(e). It can be found that the *cis*-AB content decreased and then approached asymptotically the same photo-stationary composition ($20 \pm 5\%$ of *cis*-AB) with increasing irradiation time in the four solvents at 50 °C. Compared to the photo-isomerization at room temperature, we found that the temperature has no significant influence on the photoreaction rate and the photo-isomerization equilibrium of AB, which was due to the temperature coefficient of the photochemical reactions being relatively small (close to 1).^{43,44} Therefore, in our presented cases, the heating effect is quite slight in photoinduced isomerization of AB.

Conclusions

We have presented herein how the THz-TDS technique could quantitatively monitor the thermally induced and photoinduced

isomerization processes of AB. By utilizing THz-TDS, we demonstrate that the rate of thermal *cis-to-trans* isomerization of AB in non-polar solvent is faster than that in polar solvent; and Au NPs as a catalyst can effectively promote the thermal *cis-to-trans* isomerization of AB; we also provide evidence that the solvent polarity, temperature and Au NPs as a catalyst don't affect the photo-isomerization of AB obviously. THz-TDS enables quantitative distinguishing of the conversion state from one isomer to the other that occurs in response to light or heat and thus offer new insights into the isomerization processes. Given the extraordinary sensitivity of this technology, we believe the decisive and non-destructive THz-TDS provides exciting possibilities for investigations and better understanding of the conformational dynamics of molecules.

Conflicts of interest

There are no conflicts of interest to declare.

Acknowledgements

This work was supported by the National Key Research and Development Program of China (No. 2017YFA0701004), and the National Natural Science Foundation of China (Grant No. 61875150, 61735012, 61420106006, 61427814 and 61605143).

Notes and references

- H. M. D. Bandara and S. C. Burdette, *Chem. Soc. Rev.*, 2012, **41**, 1809–1825.
- C. J. Saint-Louis, *Control of molecular geometries using new photo-electro-switchable azobenzenes*, The University of Alabama, 2015.
- G. S. Hartley, *Nature*, 1937, **140**, 281.
- M. A. Kienzler, A. Reiner, E. Trautman, S. Yoo, D. Trauner and E. Y. Isacoff, *J. Am. Chem. Soc.*, 2013, **135**, 17683–17686.
- M. Dong, A. Babalhavaejji, C. V. Collins, K. Jarrah, O. Sadvovskii, Q. Dai and G. A. Woolley, *J. Am. Chem. Soc.*, 2017, **139**, 13483–13486.
- K. G. Yager and C. J. Barrett, *J. Photochem. Photobiol.*, A, 2006, **182**, 250–261.
- Z. F. Liu, K. Hashimoto and A. Fujishima, *Nature*, 1990, **347**, 658.
- Z. Li, M. Wang, H. Li, J. He, N. Li, Q. Xu and J. Lu, *J. Mater. Chem. C*, 2017, **5**, 8593–8598.
- Y. Norikane and N. Tamaoki, *Org. Lett.*, 2004, **6**, 2595–2598.
- T. Muraoka, K. Kinbara and T. Aida, *Nature*, 2006, **440**, 512–515.
- A. A. Beharry and G. A. Woolley, *Chem. Soc. Rev.*, 2011, **40**, 4422–4437.
- M. R. Molla, P. Rangadurai, L. Antony, S. Swaminathan, J. J. de Pablo and S. Thayumanavan, *Nat. Chem.*, 2018, **10**, 659–666.
- M. Quick, A. L. Dobryakov, M. Gerecke, C. Richter, F. Berndt, I. N. Ioffe, A. A. Granovsky, R. Mahrwald, N. P. Ernsting and S. A. Kovalenko, *J. Phys. Chem. B*, 2014, **118**, 8756–8771.
- C. M. Stuart, R. R. Frontiera and R. A. Mathies, *J. Phys. Chem. A*, 2007, **111**, 12072–12080.
- R. D. Curtis, J. W. Hilborn, G. Wu, M. D. Lumsden, R. E. Wasylshen and J. A. Pincock, *J. Phys. Chem.*, 1993, **97**, 1856–1861.
- V. Jelic, K. Iwaszczuk, P. H. Nguyen, C. Rathje, G. J. Hornig, H. M. Sharum, J. R. Hoffman, M. R. Freeman and F. A. Hegmann, *Nat. Phys.*, 2017, **13**, 591–598.
- S. P. Delaney and T. M. Korter, *J. Phys. Chem. A*, 2015, **119**, 3269–3276.
- N. Goubet, A. Jagtap, C. Livache, B. Martinez, H. Portales, X. Z. Xu, R. Lobo, B. Dubertret and E. Lhuillier, *J. Am. Chem. Soc.*, 2018, **140**, 5033–5036.
- P. H. Siegel, *IEEE Trans. Microwave Theory Tech.*, 2004, **52**, 2438–2447.
- M. Naftaly and R. E. Miles, *Proc. IEEE*, 2007, **95**, 1658–1665.
- B. Fischer, M. Hoffmann, H. Helm, G. Modjesch and P. U. Jepsen, *Semicond. Sci. Technol.*, 2005, **20**, S246.
- J. Turkevich, P. C. Stevenson and J. Hillier, *Discuss. Faraday Soc.*, 1951, **11**, 55–75.
- C. J. Brown, *Acta Crystallogr.*, 1966, **21**, 146–152.
- G. C. Hampson and J. M. Robertson, *J. Chem. Soc.*, 1941, 409–413, DOI: 10.1039/JR9410000409.
- D. Grischkowsky, S. Keiding, M. van Exter and C. Fittinger, *J. Opt. Soc. Am. B*, 1990, **7**, 2006–2015.
- J. Han, Z. Zhu, S. Ray, A. K. Azad, W. Zhang, M. He, S. Li and Y. Zhao, *Appl. Phys. Lett.*, 2006, **89**, 031107.
- T. Beyer and S. L. Price, *CrystEngComm*, 2000, **2**, 183–190.
- Y. C. Shen, P. C. Upadhyaya, E. H. Linfield and A. G. Davies, *Appl. Phys. Lett.*, 2003, **82**, 2350–2352.
- M. Takahashi, N. Okamura, X. Fan, H. Shirakawa and H. Minamide, *J. Phys. Chem. A*, 2017, **121**, 2558–2564.
- T. Pan, S. Li, T. Zou, Z. Yu, B. Zhang, C. Wang, J. Zhang, M. He and H. Zhao, *Spectrochim. Acta, Part A*, 2017, **178**, 19–23.
- S. Zong, G. Ren, S. Li, B. Zhang, J. Zhang, W. Qi, J. Han and H. Zhao, *J. Mol. Struct.*, 2018, **1157**, 486–491.
- M. Walther, B. M. Fischer and P. Uhd Jepsen, *Chem. Phys.*, 2003, **288**, 261–268.
- N. Norio, S. Toshinobu, Y. Hideyuki, I. Etsuko, Y. Shunzo and H. Shigeo, *Bull. Chem. Soc. Jpn.*, 1976, **49**, 1381–1387.
- F. Serra and E. M. Terentjev, *Macromolecules*, 2008, **41**, 981–986.
- G. Angelini, N. Canilho, M. Emo, M. Kingsley and C. Gasbarri, *J. Org. Chem.*, 2015, **80**, 7430–7434.
- P. De Maria, A. Fontana, C. Gasbarri, G. Siani and P. Zanirato, *ARKIVOC*, 2009, **8**, 16–29.
- N. K. Joshi, M. Fuyuki and A. Wada, *J. Phys. Chem. B*, 2014, **118**, 1891–1899.
- G. L. Hallett-Tapley, C. D'Alfonso, N. L. Pacioni, C. D. McTiernan, M. Gonzalez-Bejar, O. Lanzalunga, E. I. Alarcon and J. C. Scaiano, *Chem. Commun.*, 2013, **49**, 10073–10075.
- S. Simoncelli and P. F. Aramendía, *Catal. Sci. Technol.*, 2015, **5**, 2110–2116.

- 40 G. S. Hammond, J. Saltiel, A. A. Lamola, N. J. Turro, J. S. Bradshaw, D. O. Cowan, R. C. Counsell, V. Vogt and C. Dalton, *J. Am. Chem. Soc.*, 1964, **86**, 3197–3217.
- 41 G. Zimmerman, L. Y. Chow and U. J. Paik, *J. Am. Chem. Soc.*, 1958, **80**, 3528–3531.
- 42 D. Shin, J. H. Kang, K.-A. Min, S. Hong and B. Hee Hong, *APL Mater.*, 2014, **2**, 092501.
- 43 W. D. Bancroft and R. P. Allen, *Proc. Natl. Acad. Sci. U. S. A.*, 1929, **15**, 445–448.
- 44 G. B. Kistiakowsky, *Proc. Natl. Acad. Sci. U. S. A.*, 1929, **15**, 194–197.